ARTICLES

Smac mimetics and innate immune stimuli synergize to promote tumor death

Shawn T Beug[1], Vera A Tang[1], Eric C LaCasse[1], Herman H Cheung[1], Caroline E Beauregard[1], Jan Brun[1], Jeffrey P Nuyens[1], Nathalie Earl[1], Martine St-Jean[1], Janelle Holbrook[1], Himika Dastidar[2], Douglas J Mahoney[2], Carolina Ilkow[3], Fabrice Le Boeuf[3], John C Bell[3,4] & Robert G Korneluk[1,4]

Smac mimetic compounds (SMC), a class of drugs that sensitize cells to apoptosis by counteracting the activity of inhibitor of apoptosis (IAP) proteins, have proven safe in phase 1 clinical trials in cancer patients. However, because SMCs act by enabling transduction of pro-apoptotic signals, SMC monotherapy may be efficacious only in the subset of patients whose tumors produce large quantities of death-inducing proteins such as inflammatory cytokines. Therefore, we reasoned that SMCs would synergize with agents that stimulate a potent yet safe "cytokine storm." Here we show that oncolytic viruses and adjuvants such as poly(I:C) and CpG induce bystander death of cancer cells treated with SMCs that is mediated by interferon beta (IFN-β), tumor necrosis factor alpha (TNF-α) and/or TNF-related apoptosis-inducing ligand (TRAIL). This combinatorial treatment resulted in tumor regression and extended survival in two mouse models of cancer. As these and other adjuvants have been proven safe in clinical trials, it may be worthwhile to explore their clinical efficacy in combination with SMCs.

Several SMCs are being evaluated in early- to mid-stage clinical trials in cancer patients[1]. SMCs are rationally designed based on the properties of Smac, an endogenous pro-apoptotic protein that, upon release from the mitochondria, binds to and antagonizes several members of the IAP family. The IAP proteins are attractive cancer therapy targets because they regulate programmed cell death in tumor cells[1]. For example, the prototypical X-linked IAP (XIAP) protein, which directly inhibits key initiator and executioner caspase proteins within every programmed cell death cascade and can thereby thwart the completion of all cell death programs, is hyperactive in many human cancers[1,2]. In addition, genetic loss of the cellular IAP proteins 1 and 2 (cIAP1 and 2), which are E3 ubiquitin ligases that primarily regulate programmed cell death signaling pathways engaged by immune cytokines[3–9], causes TNF-α, TRAIL and interleukin 1 beta (IL-1β) to become toxic to the majority of cancer cells[5–16].

An important property of SMCs is that they target several IAPs, including XIAP and the cIAPs; as such, SMC therapy intervenes at multiple distinct yet interrelated stages in the inhibition of programmed cell death. This characteristic imbues SMC therapy with two noteworthy advantages over most other molecularly targeted drugs: fewer opportunities for tumors to develop resistance, and more opportunities for synergy with existing and emerging cancer therapeutics, many of which activate pro-apoptotic pathways influenced by SMCs. For example, inflammatory cytokines such as TNF-α and IL-1β and pro-apoptotic proteins such as TRAIL potently synergize with SMC therapy in many tumor-derived cell lines *in vitro*. Therapeutic strategies aimed at increasing the abundance of these pro-apoptotic proteins in SMC-treated tumors, using approaches, in particular, that would limit the toxicities commonly associated with recombinant cytokine therapy, are thus very attractive.

TNF-α, TRAIL and dozens of other cytokines and chemokines are upregulated in response to pathogen recognition by the innate immune system[17–19]. Notably, this ancient response to microbial invaders is usually self-limiting and safe, due to stringent negative regulation that limits the strength and duration of its activity. We thus asked whether stimulating the innate immune system using pathogen mimetics would be a safe and effective strategy to generate a cytokine milieu sufficient to initiate programmed cell death in tumors treated with an SMC. We report here that nonpathogenic oncolytic viruses, as well as mimetics of microbial RNA or DNA (poly(I:C) and CpG, respectively) induce bystander killing of cancer cells treated with an SMC, and that this death depends on IFN-β, TNF-α and/or TRAIL production. Importantly, this combinatorial therapeutic strategy was tolerable *in vivo* in mice and led to durable cures in several mouse models of aggressive cancer.

RESULTS
Synergistic induction of bystander cell death
Oncolytic viruses are currently in phases 1–3 clinical evaluation in cancer patients[20]. A major barrier to effective oncolytic virus therapy is virus-induced expression of type I IFN and nuclear factor kappa B (NF-κB)-responsive cytokines, which orchestrate an antiviral state in tumors. We sought to exploit these cytokines to induce programmed cell death in cancer cells that were treated with an SMC. To begin,

Figure 1 SMC synergizes with oncolytic rhabdoviruses to induce bystander death of cancer cells. (**a**) Alamar blue viability assays of EMT6 and SNB75 cells treated with vehicle or 5 µM LCL161 (SMC) and increasing MOI of VSVΔ51 for 48 h. Error bars, mean ± s.d. $n = 4$. (**b**) Micrographs of cells treated with vehicle or 5 µM LCL161 and PBS or 0.1 MOI of VSVΔ51-GFP. Scale bars, 100 µm. (**c**) Alamar blue viability assays of cells treated with PBS or infected with 0.1 MOI of VSVΔ51 in the presence of increasing concentrations of LCL161 for 48 h. Error bars, mean ± s.d. $n = 3$. (**d**) Cells were stained with Hoechst (nucleus) and MR-DEVD (to reveal active caspase-3) cells after cotreatment with 5 µM LCL161 and 0.01 MOI of VSVΔ51-GFP for 36 h. i–iv are higher magnification images of the boxed areas. Scale bars, 100 µm. (**e**) Cells were infected with VSVΔ51 at the indicated MOI for 24 h, cell culture supernatant was exposed to virus-inactivating UV light and then supernatant was applied at indicated dilutions to new cells in the presence of vehicle or 5 µM LCL161. Alamar blue viability assays were performed 48 h after treatment. Error bars, mean ± s.d. $n = 3$. (**f**) Cells were cotreated with vehicle or 5 µM LCL161 and nonspreading virus VSVΔ51ΔG (0.1 MOI). Alamar blue viability assays were performed at 48 h after treatment. Error bars, mean ± s.d. $n = 3$. (**g**) Human renal adenocarcinoma 786-0 cells were overlaid with agarose media containing 5 µM LCL161 and inoculated with 500 PFU of VSVΔ51-GFP in the middle of the well. At 96 h post-treatment, virus infectivity was measured by fluorescence and cytotoxicity was assessed by crystal violet (CV) staining. Images were superimposed; nonsuperimposed images are in **Supplementary Figure 6**. Error bars, mean ± s.d. $n = 4$. Scale bars, 5 mm. All figure panels: representative data from at least three independent experiments using biological replicates.

we screened a small panel of tumor-derived human and mouse ($n = 28$) and normal ($n = 2$) cell lines for responsiveness to the SMC LCL161 and the oncolytic rhabdovirus vesicular stomatitis virus (VSV)Δ51. We chose LCL161 because this compound is the most clinically advanced drug in the SMC class[21–23] and VSVΔ51 because it is known to induce a robust antiviral cytokine response[24]. In 15 of the 28 tumor cell lines tested (54%), SMC treatment reduced the half-maximal effective concentration (EC50) of VSVΔ51 by 10- to 10,000-fold (**Supplementary Fig. 1** and representative examples in **Fig. 1a,b**). Similarly, low dose VSVΔ51 reduced the EC50 of SMC from undetermined levels (>2,500 nM) to 4.5 and 21.9 nM in mouse mammary carcinoma EMT6 and human glioblastoma SNB75 cells, respectively (**Fig. 1c**). Combination index analyses determined that the interaction between SMC and VSVΔ51 was synergistic (**Supplementary Fig. 2**). Experiments using four other SMCs and five other oncolytic viruses showed that all tested monomer and dimer SMCs (containing one or two IAP binding motifs, respectively) synergize with VSVΔ51 in inducing EMT6 and SNB75 cell death (**Supplementary Fig. 3**). The oncolytic rhabdoviruses VSVΔ51 and Maraba-MG1 were superior in eliciting bystander killing with SMCs compared to herpes simplex

virus (HSV), reovirus, vaccinia and wild-type VSV (**Supplementary Fig. 4**); this may be explained by the fact that the latter four viruses can use elaborate mechanisms to suppress innate immune signaling[20]. RNA interference (RNAi)-mediated silencing of XIAP and the cIAPs demonstrated that synergy with VSVΔ51 required silencing of both XIAP and the cIAPs (**Supplementary Fig. 5**). In contrast to the results in tumor-derived cell lines, noncancer GM38 primary human skin fibroblasts and human skeletal muscle myoblasts were unaffected by VSVΔ51 and SMC combination therapy (**Supplementary Fig. 1**). Taken together, these data indicate that oncolytic VSV synergized with SMC therapy specifically in tumor cells.

To determine if VSVΔ51 elicits bystander cell death in neighboring uninfected cells, we treated cells with SMCs before infection with a low dose of VSVΔ51 (multiplicity of infection (MOI) = 0.01 infectious particles per cell). Immunofluorescent colocalization analyses revealed that the majority of uninfected EMT6 cells stained positive for cleaved caspase-3 (**Fig. 1d**), a marker of apoptosis; these findings suggest the induction of widespread bystander cell death. To complement this experiment, we assessed whether conditioned media derived from cells infected with VSVΔ51 (which was subsequently

inactivated by UV light) could induce death when transferred to a plate of uninfected cancer cells treated with an SMC. The conditioned media induced cell death only when the cells were treated at the same time with an SMC (**Fig. 1e**). We also found that a low dose of a pseudotyped strain, VSVΔ51ΔG (containing a deletion of the gene encoding its glycoprotein), that limits the virus to a single round of infection, was toxic to an entire plate of cancer cells treated with an SMC (**Fig. 1f**). Finally, we performed a cytotoxicity assay in cells overlaid with agarose, which retards the spread of virus; we infected these cells with VSVΔ51 expressing a fluorescent tag[25,26], and observed death of SMC-treated cells outside of the zone of virus infection (**Fig. 1g** and **Supplementary Fig. 6**). Overall, these results indicate that VSVΔ51 infection led to the release of at least one soluble factor that potently induced bystander cell death in neighboring, uninfected cancer cells treated with SMCs.

SMCs do not suppress antiviral immunity

Mammalian cells respond to infection with an RNA virus through a signaling cascade initiated by members of a family of cytosolic (RIG-I-like receptors, RLRs) and endosomal (toll-like receptors, TLRs) viral RNA sensors[27]. Once triggered, these receptors activate IFN-response factor (IRF) 3/7 and NF-κB, which results in production of IFNs and IFN-responsive genes as well as an array of inflammatory chemokines and cytokines. This response 'warns' neighboring cells of an impending virus encounter, prompting those cells to preemptively express antiviral genes; it also promotes recruitment and activation of immune cells with the ability to clear the virus infection. Because the cIAP proteins were recently implicated in innate immune signaling pathways including those emanating from RLRs and TLRs[6,8], we asked whether SMC therapy alters the antiviral response to oncolytic VSV infection in tumor cells and in mice.

First, we evaluated the effect of SMC therapy on VSVΔ51 replication and spread. Single-step and multistep virus growth curves revealed that SMC treatment did not affect the kinetics of VSVΔ51 growth in EMT6 or SNB75 cells *in vitro* (**Fig. 2a**). Similarly, time-lapse microscopy showed that SMC treatment did not alter VSVΔ51 infectivity in or spread through tumor cells *in vitro* (**Fig. 2b**). We analyzed viral replication and spread *in vivo* by determining abundance of virus within tumor and normal tissue using an *in vivo* imaging system (IVIS) and tissue virus titration. We found no differences in the kinetics of viral spread in vehicle- or SMC-treated EMT6 tumor-bearing mice (**Supplementary Fig. 7**). These data provide indirect evidence that SMC treatment did not markedly affect the antiviral response of cancer and normal cells.

To directly analyze the antiviral response, we measured IFN-β production in EMT6 and SNB75 cells treated with VSVΔ51 and SMCs. SMC-treated cancer cells responded to VSVΔ51 by secreting IFN-β (**Fig. 2c**), although in slightly lower amounts than vehicle-treated cancer cells. However, quantitative RT-PCR analysis of a small panel of IFN-stimulated genes (ISGs) in cells treated with VSVΔ51 and vehicle or SMC revealed that SMC treatment did not markedly affect ISG gene expression (**Fig. 2d**). Consistent with this finding, western blot analyses indicated that SMC treatment did not alter IFN-β-induced STAT1 phosphorylation (**Fig. 2e**). Finally, an IFN bioassay was used to measure the extent of protection of cells against cytopathic wild-type VSV. Supernatants obtained from EMT6 cells that were pretreated with SMC and VSVΔ51 provided protection against virus-induced cell death (**Fig. 2f**), thus demonstrating that SMC therapy did not alter the capacity of tumor cells to generate an antiviral response upon VSVΔ51 infection. Collectively, these data demonstrate that SMCs did not impede the ability of tumor cells to sense and respond to infection with VSVΔ51.

Mechanisms of bystander cell death

We previously showed that SMCs sensitize a number of cancer cell lines toward caspase-8-dependent apoptosis induced by TNF-α, TRAIL and IL-1β[15,16]. As RNA viruses trigger the production of these cytokines, we investigated the involvement of cytokine signaling in death induced by combinatorial treatment with SMC and oncolytic virus. First, we treated cells with short interfering RNA (siRNA) specific for the TNF receptor TNF-R1 and/or the TRAIL receptor DR5. This experiment revealed that TNF-α and TRAIL were indispensable for bystander cell death induced by SMC and VSVΔ51 (**Fig. 3a** and **Supplementary Fig. 8a**). Western blot and immunofluorescence experiments revealed strong activation of the extrinsic apoptosis pathway; consistent with this, RNAi knockdown of caspase-8 and Rip1 revealed roles for these proteins in the bystander cell death induced by SMC and VSVΔ51 (**Supplementary Fig. 9**). VSVΔ51, engineered to express TNF-α, boosted cell death by an order of magnitude (**Supplementary Fig. 10**), further solidifying a role for this cytokine in the efficacy of SMCs.

Next we silenced the type I IFN receptor (IFNAR1) and found, quite unexpectedly, that IFNAR1 knockdown prevented the synergy between SMC therapy and oncolytic VSV (**Fig. 3b** and **Supplementary Fig. 8b**). We predicted that IFNAR1 knockdown would dampen bystander killing, as TRAIL is a well-established ISG downstream of type I IFN signaling[28]. However, as TNF-α and IL-1β are considered to be independent of IFN signaling (although responsive to NF-κB signaling downstream of virus detection), we predicted that IFNAR1 knockdown would not completely suppress bystander killing[29]. This result suggests the possibility of a noncanonical type I, IFN-dependent pathway regulating the production of TNF-α and/or IL-1β. Indeed, when we measured expression of transcripts encoding IFN-β, TRAIL, TNF-α and IL-1β during an oncolytic VSV infection, we found a significant temporal lag between the induction of IFN-β and that of both TRAIL and TNF-α (**Fig. 3c**). These data also suggest that TNF-α—like TRAIL—may be induced secondarily to IFN-β. To test this hypothesis, we treated cells with IFNAR1 siRNA before treating them with VSVΔ51. IFNAR1 knockdown completely abrogated the VSVΔ51-induced expression of both TRAIL and TNF-α (**Fig. 3d**). Moreover, recombinant type I (IFN-α/β) or type II IFN (IFN-γ), but not type III IFN (IL28/29), effectively substituted for VSVΔ51 in synergizing with SMC to induce bystander killing (**Fig. 3e**).

To further explore this noncanonical pathway leading to induction of TNF-α and TRAIL, we measured TRAIL and TNF-α mRNA expression in SNB75 cells treated with recombinant IFN-β. Both cytokines were induced by IFN-β treatment (**Fig. 3f**) and enzyme-linked immunosorbent (ELISA) experiments confirmed the production of their respective protein products in the cell culture media (**Fig. 3g**). Interestingly, there was a significant time lag between the induction of TRAIL and that of TNF-α. As TRAIL is a bona fide ISG and TNF-α is not, this result raised the possibility that TNF-α is not induced by IFN-β directly, but responds to a downstream ISG upregulated by IFN-β. We thus performed quantitative RT-PCR on 176 cytokines in SNB75 cells and identified 70 that displayed a three-fold increase of gene expression by IFN-β treatment (**Supplementary Table 1**). We are currently investigating the potential roles of these ISGs in the induction of TNF-α by IFN-β. Notably, SMC treatment potentiated the induction of both TRAIL and TNF-α by IFN-β in SNB75 cells (**Fig. 3f,g**). For example, in EMT6 cells, SMC treatment enhanced VSV-induced TNF-α production by five- to sevenfold (**Supplementary Fig. 11**). Furthermore, using a dominant-negative construct of IKK, we found that the production of these inflammatory cytokines downstream of IFN-β was dependent, at least in part, on classical NF-κB signaling (**Fig. 3h**). Finally, blocking TNF-R1 signaling
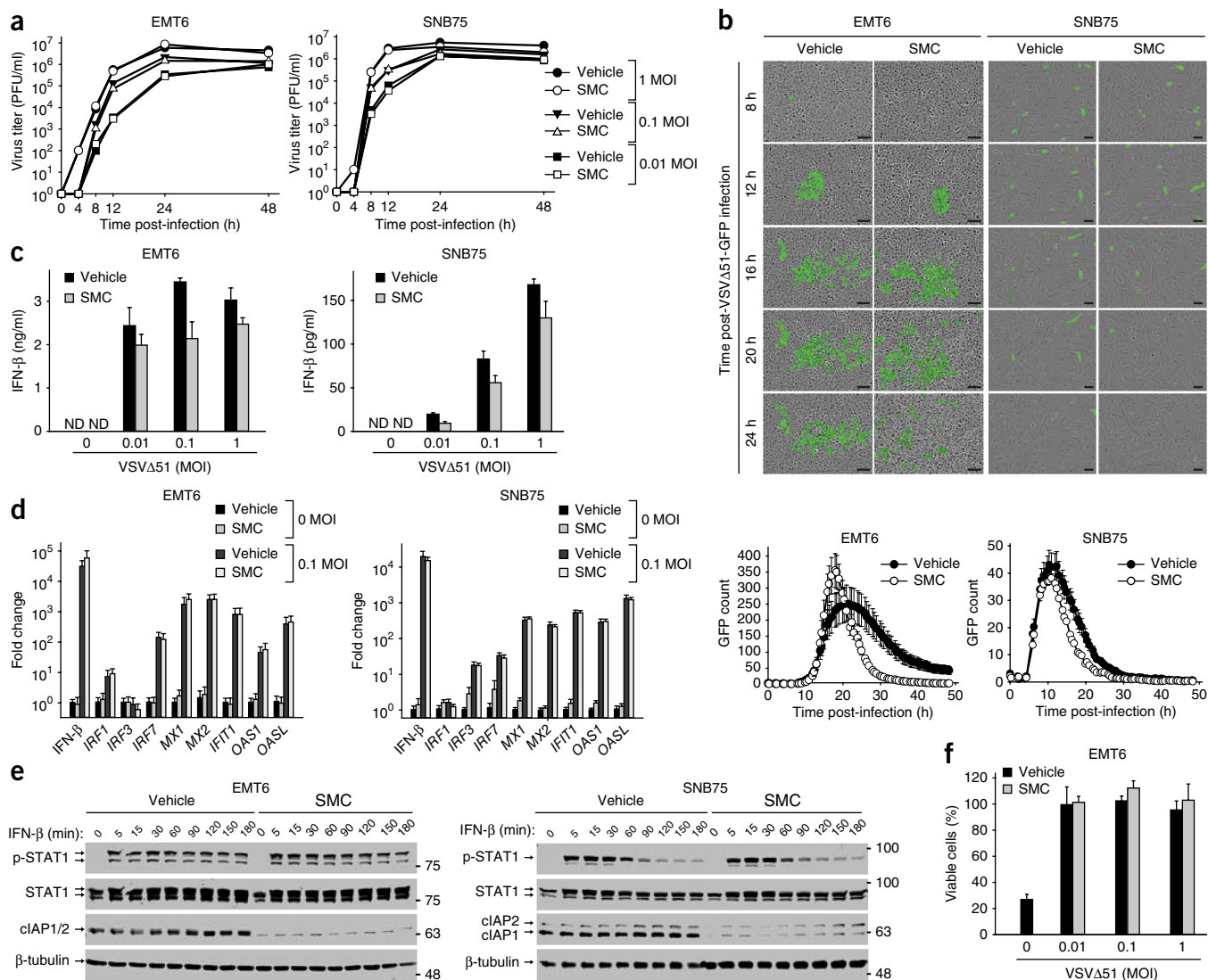
Figure 2 SMC treatment does not alter the antiviral response of cancer cells. (**a**) Cells were pretreated with vehicle or 5 μM LCL161 (SMC) for 2 h and infected with the indicated MOI of VSVΔ51. At indicated time points, virus titer was assessed by a standard plaque assay. Error bars, mean ± s.d. (**b**) Cells were treated with vehicle or 5 μM LCL161 and infected with VSVΔ51-GFP (0.1 MOI). Cells were imaged every 30 min using the Incucyte Zoom. Images are representative of four experiments and graphs below images show the number of GFP signals detected at each time point. Error bars, mean ± s.d. $n = 12$. Scale bars, 100 μm. (**c**) Cell culture supernatants from cells treated with vehicle or 5 μM LCL161 and indicated MOI of VSVΔ51 for 24 h were processed for the presence of IFN-β by ELISA. Error bars, mean ± s.d. $n = 3$. ND, not detected. (**d**) Cells were treated with vehicle or 5 μM LCL161 and indicated MOI of VSVΔ51 for 20 h. Cells were then processed for RT-qPCR to measure expression of virus and IFN-stimulated gene transcripts indicated on the x axis. Error bars, mean ± s.d. $n = 3$. (**e**) Cells were pretreated with 5 μM LCL161 for 2 h and subsequently stimulated with IFN-β for the indicated times. Total and phosphorylated STAT1, cIAP1/2 knockdown and β-tubulin (loading control) was measured by western blot analysis. (**f**) EMT6 cells were treated with vehicle or 5 μM LCL161 and infected with the indicated MOI of VSVΔ51 for 20 h. Media was exposed to UV light and then applied to uninfected cells. Cells were subsequently challenged with 1 MOI of wild-type VSV for 48 h and the proportion of rescue of cell death from wild-type VSV was measured by an Alamar blue viability assay. Error bars, mean ± s.d. $n = 3$. All figure panels: representative data from at least three independent experiments using biological replicates.

(with antibodies or siRNA) prevented EMT6 cell death in the presence of SMC and VSVΔ51 or IFN-β (**Supplementary Fig. 12**).

In vivo synergistic effects

To evaluate SMC and oncolytic VSV co-therapy *in vivo*, we first used the EMT6 mammary carcinoma as a syngeneic, orthotopic model. Preliminary safety and pharmacodynamic experiments revealed that a dose of 50 mg/kg LCL161 delivered by oral gavage was well tolerated by mice (transient loss of ~5% body weight that is recovered within 5 d) and induced cIAP1/2 knockdown in tumors for at least 24 h, and up to 48–72 h in some cases. The reduction in XIAP levels

was not as pronounced (**Supplementary Fig. 13**). When tumors reached ~100 mm³, we began treating mice twice weekly with vehicle or 50 mg/kg LCL161 (oral) and/or 5×10^8 plaque-forming units (PFU) VSVΔ51 (intravenous (i.v.)). LCL161 therapy alone decreased the rate of tumor growth and modestly extended survival, whereas VSVΔ51 alone did not markedly alter tumor growth or mouse survival (**Fig. 4a,b**). However, combined SMC and VSVΔ51 treatment induced tumor regression and led to durable cures in 40% of the treated mice. Consistent with the bystander killing mechanism elucidated *in vitro*, immunofluorescence analyses revealed that the infectivity of VSVΔ51 was transient and limited to small foci within the tumor (**Fig. 4c**),
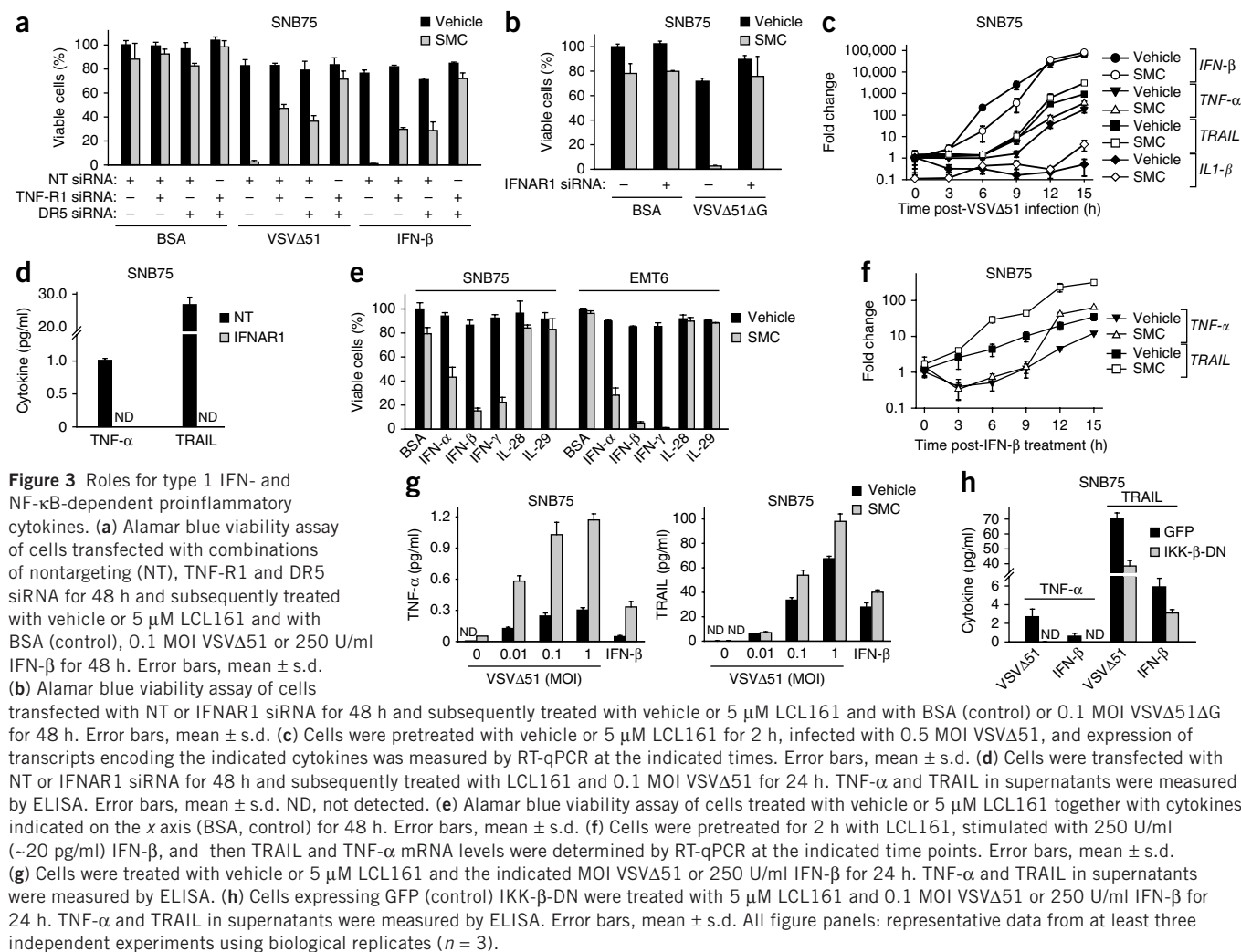
Figure 3 Roles for type 1 IFN- and NF-κB-dependent proinflammatory cytokines. (**a**) Alamar blue viability assay of cells transfected with combinations of nontargeting (NT), TNF-R1 and DR5 siRNA for 48 h and subsequently treated with vehicle or 5 µM LCL161 and with BSA (control), 0.1 MOI VSVΔ51 or 250 U/ml IFN-β for 48 h. Error bars, mean ± s.d. (**b**) Alamar blue viability assay of cells transfected with NT or IFNAR1 siRNA for 48 h and subsequently treated with vehicle or 5 µM LCL161 and with BSA (control) or 0.1 MOI VSVΔ51ΔG for 48 h. Error bars, mean ± s.d. (**c**) Cells were pretreated with vehicle or 5 µM LCL161 for 2 h, infected with 0.5 MOI VSVΔ51, and expression of transcripts encoding the indicated cytokines was measured by RT-qPCR at the indicated times. Error bars, mean ± s.d. (**d**) Cells were transfected with NT or IFNAR1 siRNA for 48 h and subsequently treated with LCL161 and 0.1 MOI VSVΔ51 for 24 h. TNF-α and TRAIL in supernatants were measured by ELISA. Error bars, mean ± s.d. ND, not detected. (**e**) Alamar blue viability assay of cells treated with vehicle or 5 µM LCL161 together with cytokines indicated on the x axis (BSA, control) for 48 h. Error bars, mean ± s.d. (**f**) Cells were pretreated for 2 h with LCL161, stimulated with 250 U/ml (~20 pg/ml) IFN-β, and then TRAIL and TNF-α mRNA levels were determined by RT-qPCR at the indicated time points. Error bars, mean ± s.d. (**g**) Cells were treated with vehicle or 5 µM LCL161 and the indicated MOI VSVΔ51 or 250 U/ml IFN-β for 24 h. TNF-α and TRAIL in supernatants were measured by ELISA. (**h**) Cells expressing GFP (control) IKK-β-DN were treated with 5 µM LCL161 and 0.1 MOI VSVΔ51 or 250 U/ml IFN-β for 24 h. TNF-α and TRAIL in supernatants were measured by ELISA. Error bars, mean ± s.d. All figure panels: representative data from at least three independent experiments using biological replicates (n = 3).

whereas caspase-3 activation was widespread in tumors cotreated with SMC and VSVΔ51 (**Fig. 4d**). Furthermore, western blots of tumor lysates demonstrated activation of caspase-8 and caspase-3 in double-treated tumors (**Fig. 4e**). Although the animals in the combination treatment cohort lost weight, the mice fully recovered after the last treatment (**Supplementary Fig. 14a**).

To confirm these *in vivo* data in another model system, we tested the human HT-29 colorectal adenocarcinoma xenograft model in nude (athymic) mice. HT-29 is a cell line that is highly responsive to bystander killing by SMC and VSVΔ51 cotreatment *in vitro* (**Supplementary Fig. 15a**,**b**). Similar to our findings in the EMT6 model system, combination therapy with 50 mg/kg LCL161 (oral) and 1 ×10^{8} PFU (intratumoral) of VSVΔ51 slowed tumor growth and led to a significant extension of mouse survival (**Supplementary Fig. 15c**). In contrast, neither monotherapy had any effect on HT-29 tumors. Furthermore, there was no additional weight loss in the double-treated mice compared to SMC-treated mice (**Supplementary Fig. 15d**). These results in the HT-29 model indicate that the synergy between SMC and VSVΔ51 does not completely require the adaptive immune response.

Next, we wished to determine whether oncolytic virus infection coupled with SMC treatment leads to TNF-α- and/or IFN-β-mediated cell death *in vivo*. Compared to an isotype control antibody, TNF-α neutralizing antibody prevented SMC and VSVΔ51-induced EMT6

tumor regression and mouse survival extension (**Fig. 4f**,**g**). However, treatment of BALB/c mice bearing EMT6 tumors with IFNAR1-blocking antibodies resulted in mouse death due to viremia within 24–48 h after infection. Nevertheless, before mouse death and 18–20 h after virus infection, we collected tumors and analyzed caspase activity. Compared to SMC and VSVΔ51-treated mice injected with isotype control antibody, those injected with anti-IFNAR1 showed no caspase-8 activity and much less caspase-3 activity (**Supplementary Fig. 16**). These results support the hypothesis that intact TNF-α and type I IFN signaling was required to mediate the *in vivo* anti-tumor effects of the combinatorial treatment.

To assess the contribution of innate immune cells or other immune mediators to the efficacy of combination therapy, we first attempted to treat EMT6 tumors in immunodeficient non-obese–severe combined immune deficiency (NOD-SCID) or NSG (NOD-scid-IL2Rgamma[null]) mice. However, similar to mice treated with anti-IFNAR1, these mice died rapidly due to viremia (data not shown). Therefore, we addressed the contribution of innate immune cells in an *ex vivo* splenocyte culture system. Sorted splenic macrophages (CD11b^{+} F4/80^{+}), neutrophils (CD11b^{+} Gr1^{+}), natural killer (NK) cells (CD11b^{−} CD49b^{+}) and nonmyeloid (CD11b^{−} CD49^{−}) populations were stimulated with VSVΔ51, and the conditioned medium was transferred to EMT6 cells treated with vehicle or SMC. VSVΔ51-stimulated macrophages and neutrophils, but not NK cells,

produced factors that led to cancer cell death in the presence of SMCs (**Supplementary Fig. 17a**). We also isolated primary macrophages from bone marrow and these macrophages also responded to oncolytic VSV infection in a dose-dependent manner to produce factors

that kill EMT6 cells (**Supplementary Fig. 17b**). Altogether, these findings demonstrate that multiple innate immune cell populations can mediate the observed anti-tumor effects, but that macrophages may be the most likely effectors of this response.
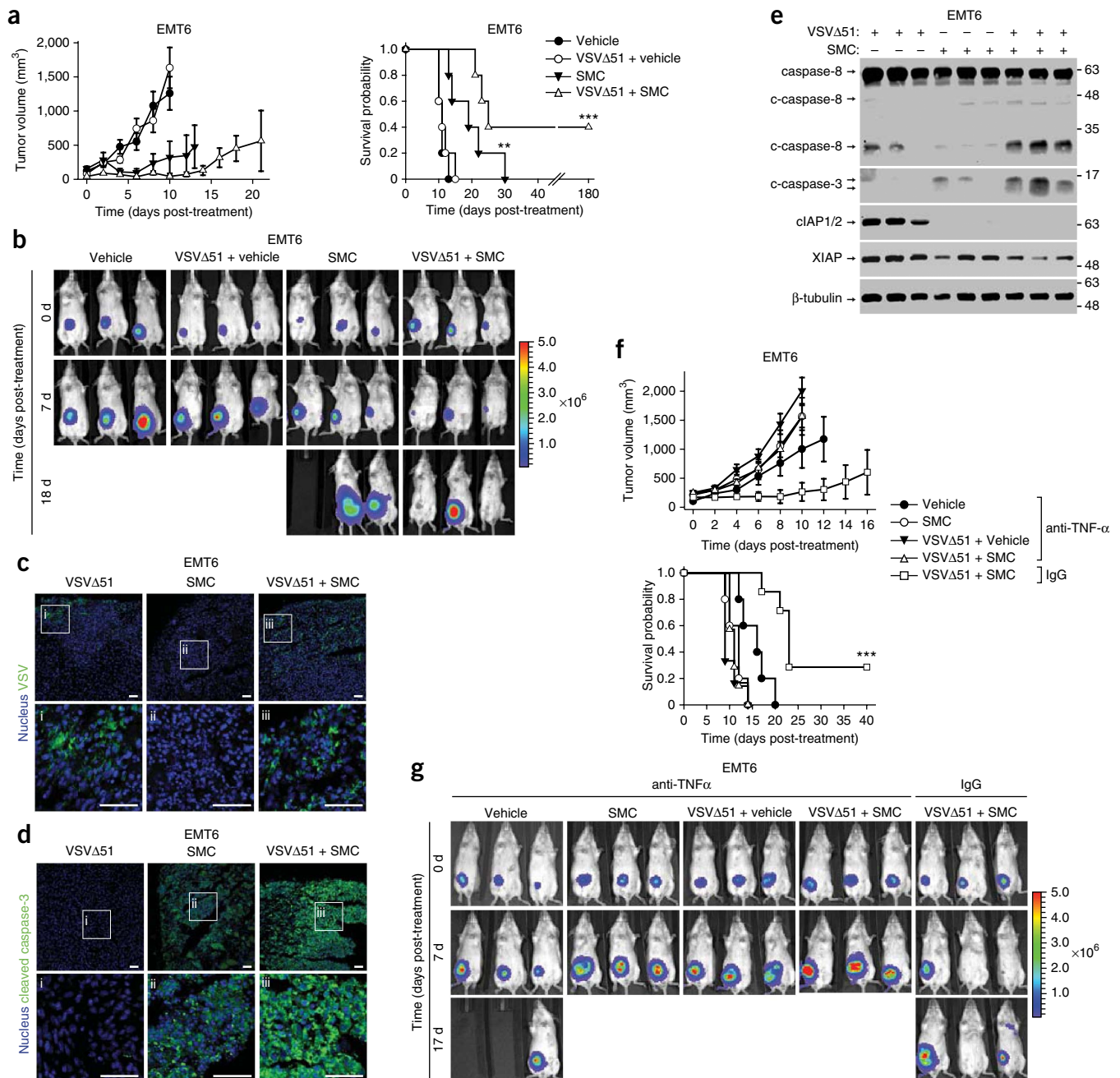
Figure 4 Combinatorial SMC and oncolytic virus treatment is efficacious *in vivo* and depends on cytokine signaling. (**a**) Mice bearing ~100 mm³ EMT6-Fluc tumors were treated with vehicle or with 50 mg/kg LCL161 (SMC) (oral) and/or 5 × 10⁸ PFU VSVΔ51 (i.v.). Left panel depicts tumor growth. Right panel represents the Kaplan-Meier curve depicting mouse survival. Error bars, mean ± s.e.m. *n* = 5 per group. Log-rank with Holm-Sidak multiple comparison: **P < 0.01; ***P < 0.001. Representative data from two independent experiments. (**b**) Representative IVIS images from mice described in **a** were acquired at indicated time points. Scale: p/sec/cm²/sr. (**c,d**) 24 h after treatment as in **a**, tumors were isolated and analyzed by immunofluorescence using VSV (**c**) or cleaved caspase-3-specific (**d**) antibodies. i–iii are higher magnification images of the boxed areas in the top row. Scale bars 50 μm. Representative data from two experiments. (**e**) Lysates of tumors from mice treated for 20 h as in **a** were blotted with the indicated antibodies. Representative data from two experiments. (**f**) Mice bearing ~100 mm³ EMT6-Fluc tumors were treated with neutralizing TNF-α antibody or isotype control (IgG) antibody and subsequently treated with 50 mg/kg LCL161 (oral) and/or 5 × 10⁸ PFU VSVΔ51 (i.v.). Top panel depicts tumor growth. Bottom panel represents the Kaplan-Meier curve depicting mouse survival. Error bars, mean ± s.e.m. Vehicle α-TNF-α, *n* = 5; SMC α-TNF-α, *n* = 5; vehicle+VSVΔ51, *n* = 5; α-TNF-α, *n* = 5; SMC+VSVΔ51 α-TNF-α, *n* = 7; SMC+VSVΔ51 IgG, *n* = 7. Log-rank with Holm-Sidak multiple comparison: ***, P < 0.001. (**g**) Representative IVIS images from mice from **f**. Scale: p/sec/cm²/sr.

Adjuvants potentiate SMC effects *in vivo*

We next investigated whether synthetic TLR agonists (often used as adjuvants) known to induce an innate proinflammatory response could replace oncolytic virus and synergize with SMCs. We co-cultured EMT6 cells with mouse splenocytes in a transwell insert system, and treated the splenocytes with SMC and agonists of TLR 3, 4, 7 or 9. All of the tested TLR agonists induced the bystander death of SMC-treated EMT6 cells (**Fig. 5a**). The TLR4, 7 and 9 agonists LPS, imiquimod and CpG, respectively, required splenocytes to induce bystander killing of EMT6 cells, presumably because their target TLR receptors

are not expressed in EMT6 cells. However, the TLR3 agonist poly(I:C) led to EMT6 cell death in the absence of splenocytes.

We next tested poly(I:C) and CpG in combination with SMC therapy *in vivo*. We chose these adjuvants as they have proven to be safe in humans and are currently being evaluated in numerous mid- to late-stage clinical trials for cancer[30–33]. EMT6 tumors were established and treated as described above. Whereas poly(I:C) treatment had no bearing on tumor growth as a single agent, when combined with SMCs it induced substantial tumor regression and, when delivered intraperitoneally, led to durable cures in 60% of the treated mice
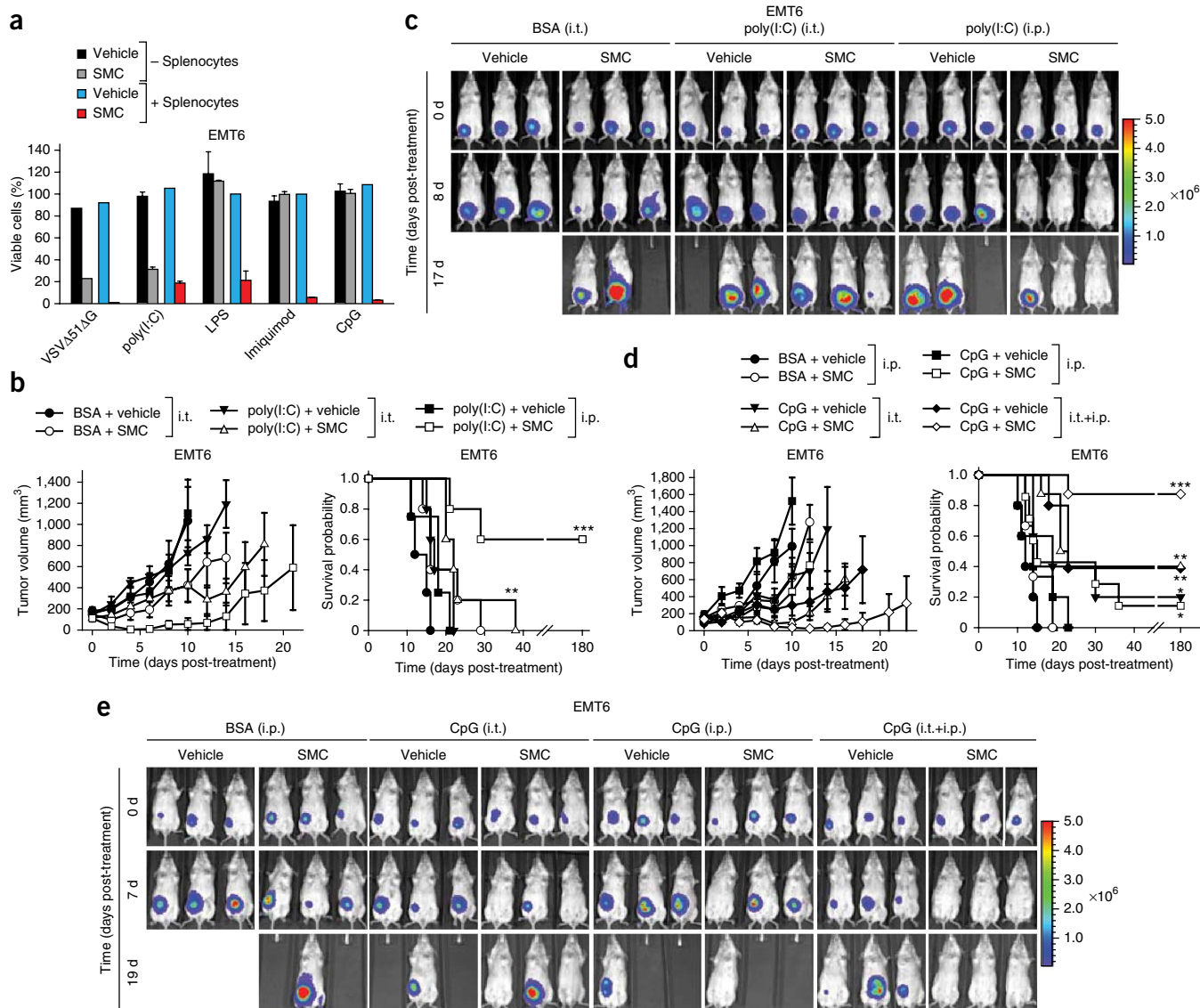
Figure 5 Adjuvants synergize with SMC therapy in murine cancer models. (**a**) Alamar blue viability assays of EMT6 cells, which were cocultured or not with splenocytes in a transwell system, and for which the segregated splenocytes were treated with vehicle or 1 µM LCL161 (SMC) and 0.1 MOI VSVΔ51ΔG (positive control) or the indicated TLR agonists (1 µg/ml poly(I:C) (TLR3), 1 µg/ml LPS (TLR4), 2 µM imiquimod (TLR7), 0.25 µM CpG (TLR9)) for 24 h. Error bars, mean ± s.d. Representative data from three independent experiments using biological replicates (*n* = 3). (**b**) Mice with established EMT6-Fluc tumors (~100 mm^3) were treated with LCL161 (50 mg/kg LCL161, oral) and poly(I:C) (15 µg intratumoral (i.t.) or 2.5 mg/kg intraperitoneal (i.p.)). Left panel depicts tumor growth. Right panel represents the Kaplan-Meier curve depicting mouse survival. Vehicle, vehicle+poly(I:C) i.p., *n* = 4; remaining groups, *n* = 5. Error bars, mean ± s.e.m. Log-rank with Holm-Sidak multiple comparison: **, *P* < 0.01; ***, *P* < 0.001. (**c**) Representative IVIS images from mice treated in **b**. Scale: p/sec/cm^2/sr. (**d**) Mice with established EMT6-Fluc tumors (~100 mm^3) were treated with 50 mg/kg LCL161 (oral) alone or in combination with 200 µg (i.t.) and/or 2.5 mg/kg (i.p.) CpG ODN 2216. Left panel depicts tumor growth. Right panel represents the Kaplan-Meier curve depicting mouse survival. Vehicle, *n* = 5; SMC, *n* = 5; vehicle+CpG i.p., *n* = 5; SMC+CpG i.p., *n* = 7; vehicle+CpG i.t., *n* = 5; SMC+CpG i.t., *n* = 8; vehicle+CpG i.p.+i.t., *n* = 5; SMC+CpG i.p.+i.t., *n* = 8. Error bars, mean ± s.e.m. Log-rank with Holm-Sidak multiple comparison: *, *P* < 0.05; **, *P* < 0.01; ***, *P* < 0.001. (**e**) Representative IVIS images from mice treated as in **d**. Scale: p/sec/cm^2/sr.

(**Fig. 5b,c**). Whereas CpG monotherapy moderately reduced tumor growth and extended survival, when combined with SMC treatment, a significant regression in tumor growth and an increase in durable cures were observed in 88% of the treated mice (**Fig. 5d,e**). Markedly, the most effective therapy was with the combination of SMC with local (intratumoral) and systemic (i.v.) administration of CpG, presumably because of the increased concentration of proinflammatory cytokines within the tumor milieu. Importantly, these combination therapies were well tolerated by the mice, and their body weight returned to pretreatment levels shortly after the cessation of therapy (**Supplementary Fig. 14b,c**). Together these data demonstrate that a series of clinically advanced innate immune adjuvants strongly and safely synergize with SMC therapy *in vivo*.

DISCUSSION

SMC medicines are rapidly progressing through clinical evaluation; however, SMCs will likely require rationally designed therapeutic partners to be maximally effective[1]. Here we demonstrate a new strategy for boosting the efficacy of SMC therapy, specifically the stimulation of a host innate immune response. Our approach is broadly useful in that it works with different SMCs and a number of pathogen mimetics in a large percentage of examined tumor cell lines. In addition, this combinatorial approach was efficacious in various aggressive, treatment-refractory, murine tumor models. Several of the SMCs studied here are in early- to mid-stage clinical evaluation and all of the pathogen mimetics/adjuvants examined here are currently in phase 1–3 clinical trials[23,30–35]. Data from the human studies have indicated that each of these medicines is safe[23,34,35], but none appear to be particularly effective as monotherapies. Our strategy overcomes the limitations of both Smac and pathogen mimetics as single agents, at least in cell-based and murine model systems.

Type I IFNs, including the therapeutically relevant cytokines IFN-α and IFN-β, were effectors of SMC-induced tumor killing. This unexpected discovery will ultimately shed light on IFN biology and death pathways involving caspase-8, which are controlled by the cIAPs and XIAP, and which can now be further explored and exploited therapeutically in combination with SMCs. The relationship between type I IFN and TNF-α is complex, as these two cytokines have complementary or opposing effects depending on the biological context[36,37]. However, in the context of SMC plus oncolytic virus treatment, a simple working model can be proposed (**Supplementary Fig. 18**). Tumor cells infected by an oncolytic RNA virus upregulate type I IFN, and this process is not affected by SMC antagonism of the IAP proteins. Those IFNs in turn signal to the same cancer cell (autocrine) and neighboring uninfected cancer cells (paracrine) and induce secretion of TNF-α and TRAIL; this process is enhanced by SMC treatment. In the presence of SMC and the cytokines TNF-α and/or TRAIL, bystander tumor cells undergo caspase-8-dependent apoptosis.

Previous work indicated that an SMC can enhance the adaptive immune response against a B16 melanoma tumor by boosting cancer vaccine–induced T-cell activity[3,4]. In contrast, our findings underscore the critical role that the innate immune response plays in this combination approach. Furthermore, although many other approaches to improve SMC therapy have been attempted, very rarely have complete responses been observed, particularly in aggressive tumors in immunocompetent mice. The one exception was cotreatment with SMC and recombinant TRAIL, which led to durable cures in at least one mouse model system[38]. We suspect that using a pathogen mimetic, whose mechanism of action is partially dependent on TRAIL, is a superior approach for two reasons. First, this approach also induces TNF-α-mediated apoptosis and necroptosis, and given the plasticity and heterogeneity of most advanced cancers, simultaneously inducing multiple distinct cell death mechanisms is more likely to be effective for treating these diseases, and resistance is less likely to develop to such treatment. Second, pathogen mimetics elicit an integrated innate immune response that includes layers of negative feedback. We suspect that these feedback mechanisms act to temper the cytokine response in ways that are difficult to replicate using recombinant proteins, and thus act as a safeguard to prevent toxicity of this combination therapy.

METHODS

Methods and any associated references are available in the online version of the paper.

Note: Any Supplementary Information and Source Data files are available in the online version of the paper.

AUTHOR CONTRIBUTIONS
S.T.B., E.C.L., V.A.T., F.L.B., D.J.M. and R.G.K. designed the experiments. S.T.B., H.H.C., J.P.N., N.E., M.S.-J., J.H., C.E.B., V.A.T., F.L., C.I., H.D. and J.B. conducted experiments. S.T.B., E.C.L., V.A.T., J.C.B., D.J.M. and R.G.K. wrote the manuscript.

COMPETING FINANCIAL INTERESTS
The authors declare competing financial interests: details are available in the online version of the paper.

Reprints and permissions information is available online at http://www.nature.com/reprints/index.html.

1. Fulda, S. & Vucic, D. Targeting IAP proteins for therapeutic intervention in cancer. *Nat. Rev. Drug Discov.* **11**, 109–124 (2012).
2. LaCasse, E.C. Pulling the plug on a cancer cell by eliminating XIAP with AEG35156. *Cancer Lett.* **332**, 215–224 (2013).
3. Dougan, M. *et al.* IAP inhibitors enhance co-stimulation to promote tumour immunity. *J. Exp. Med.* **207**, 2195–2206 (2010).
4. Vanneman, M. & Dranoff, G. Combining immunotherapy and targeted therapies in cancer treatment. *Nat. Rev. Cancer* **12**, 237–251 (2012).
5. Gyrd-Hansen, M. & Meier, P. IAPs: from caspase inhibitors to modulators of NF-kappaB, inflammation and cancer. *Nat. Rev. Cancer* **10**, 561–574 (2010).
6. Vandenabeele, P. & Bertrand, M.J. The role of the IAP E3 ubiquitin ligases in regulating pattern-recognition receptor signalling. *Nat. Rev. Immunol.* **12**, 833–844 (2012).
7. Varfolomeev, E. *et al.* Cellular inhibitors of apoptosis are global regulators of NF-kappaB and MAPK activation by members of the TNF family of receptors. *Sci. Signal.* **5**, ra22 (2012).
8. Beug, S.T., Cheung, H.H., LaCasse, E.C. & Korneluk, R.G. Modulation of immune signalling by inhibitors of apoptosis. *Trends Immunol.* **33**, 535–545 (2012).
9. Mahoney, D.J. *et al.* Both cIAP1 and cIAP2 regulate TNFalpha-mediated NF-kappaB activation. *Proc. Natl. Acad. Sci. USA* **105**, 11778–11783 (2008).
10. Li, L. *et al.* A small molecule Smac mimic potentiates TRAIL- and TNF{alpha}-mediated cell death. *Science* **305**, 1471–1474 (2004).
11. Varfolomeev, E. *et al.* IAP antagonists induce autoubiquitination of c-IAPs, NF-kappaB activation, and TNFalpha-dependent apoptosis. *Cell* **131**, 669–681 (2007).
12. Vince, J.E. *et al.* IAP antagonists target cIAP1 to induce TNFalpha-dependent apoptosis. *Cell* **131**, 682–693 (2007).

13. Petersen, S.L. *et al.* Autocrine TNFalpha signalling renders human cancer cells susceptible to Smac-mimetic-induced apoptosis. *Cancer Cell* **12**, 445–456 (2007).

14. Gaither, A. *et al.* A Smac mimetic rescue screen reveals roles for inhibitor of apoptosis proteins in tumour necrosis factor-alpha signalling. *Cancer Res.* **67**, 11493–11498 (2007).

15. Cheung, H.H., Mahoney, D.J., Lacasse, E.C. & Korneluk, R.G. Down-regulation of c-FLIP Enhances death of cancer cells by smac mimetic compound. *Cancer Res.* **69**, 7729–7738 (2009).

16. Cheung, H.H. *et al.* Smac mimetic compounds potentiate interleukin-1 beta-mediated cell death. *J. Biol. Chem.* **285**, 40612–40623 (2010).

17. Kawai, T. & Akira, S. The role of pattern-recognition receptors in innate immunity: update on Toll-like receptors. *Nat. Immunol.* **11**, 373–384 (2010).

18. Chen, G., Shaw, M.H., Kim, Y.G. & Nunez, G. NOD-like receptors: role in innate immunity and inflammatory disease. *Annu. Rev. Pathol.* **4**, 365–398 (2009).

19. McFadden, G., Mohamed, M.R., Rahman, M.M. & Bartee, E. Cytokine determinants of viral tropism. *Nat. Rev. Immunol.* **9**, 645–655 (2009).

20. Russell, S.J., Peng, K.W. & Bell, J.C. Oncolytic virotherapy. *Nat. Biotechnol.* **30**, 658–670 (2012).

21. Houghton, P.J. *et al.* Initial testing (stage 1) of LCL161, a SMAC mimetic, by the Pediatric Preclinical Testing Program. *Pediatr. Blood Cancer* **58**, 636–639 (2012).

22. Chen, K.F. *et al.* Inhibition of Bcl-2 improves effect of LCL161, a SMAC mimetic, in hepatocellular carcinoma cells. *Biochem. Pharmacol.* **84**, 268–277 (2012).

23. Dhuria, S. *et al.* Time-dependent inhibition and induction of human cytochrome P4503A4/5 by an Oral IAP Antagonist, LCL161, *in vitro* and *in vivo* in healthy subjects. *J. Clin. Pharmacol.* **53**, 642–653 (2013).

24. Breitbach, C.J. *et al.* Targeted inflammation during oncolytic virus therapy severely compromises tumour blood flow. *Mol. Ther.* **15**, 1686–1693 (2007).

25. Vaha-Koskela, M.J. *et al.* Resistance to two heterologous neurotropic oncolytic viruses, Semliki Forest virus and vaccinia virus, in experimental glioma. *J. Virol.* **87**, 2363–2366 (2013).

26. Le Boeuf, F. *et al.* Model-based rational design of an oncolytic virus with improved therapeutic potential. *Nat. Commun.* **4**, 1974 (2013).

27. Kawai, T. & Akira, S. Innate immune recognition of viral infection. *Nat. Immunol.* **7**, 131–137 (2006).

28. Kirshner, J.R., Karpova, A.Y., Kops, M. & Howley, P.M. Identification of TRAIL as an interferon regulatory factor 3 transcriptional target. *J. Virol.* **79**, 9320–9324 (2005).

29. Bose, S., Kar, N., Maitra, R., DiDonato, J.A. & Banerjee, A.K. Temporal activation of NF-kappaB regulates an interferon-independent innate antiviral response against cytoplasmic RNA viruses. *Proc. Natl. Acad. Sci. USA* **100**, 10890–10895 (2003).

30. Rosenfeld, M.R. *et al.* A multi-institution phase II study of poly-ICLC and radiotherapy with concurrent and adjuvant temozolomide in adults with newly diagnosed glioblastoma. *Neuro-oncol.* **12**, 1071–1077 (2010).

31. Butowski, N. *et al.* A phase II clinical trial of poly-ICLC with radiation for adult patients with newly diagnosed supratentorial glioblastoma: a North American Brain Tumour Consortium (NABTC01–05). *J. Neurooncol.* **91**, 175–182 (2009).

32. Butowski, N. *et al.* A North American brain tumour consortium phase II study of poly-ICLC for adult patients with recurrent anaplastic gliomas. *J. Neurooncol.* **91**, 183–189 (2009).

33. Krieg, A.M. CpG still rocks! Update on an accidental drug. *Nucleic Acid Ther.* **22**, 77–89 (2012).

34. Erickson, R.I. *et al.* Toxicity profile of small-molecule IAP antagonist GDC-0152 is linked to TNF-alpha pharmacology. *Toxicol. Sci.* **131**, 247–258 (2013).

35. Wong, H. *et al.* Dogs are more sensitive to antagonists of inhibitor of apoptosis proteins than rats and humans: a translational toxicokinetic/toxicodynamic analysis. *Toxicol. Sci.* **130**, 205–213 (2012).

36. Cantaert, T., Baeten, D., Tak, P.P. & van Baarsen, L.G. Type I IFN and TNFalpha cross-regulation in immune-mediated inflammatory disease: basic concepts and clinical relevance. *Arthritis Res. Ther.* **12**, 219 (2010).

37. Yarilina, A. & Ivashkiv, L.B. Type I interferon: a new player in TNF signalling. *Curr. Dir. Autoimmun.* **11**, 94–104 (2010).

38. Lu, J. *et al.* Therapeutic potential and molecular mechanism of a novel, potent, nonpeptide, smac mimetic SM-164 in combination with TRAIL for cancer treatment. *Mol. Cancer Ther.* **10**, 902–914 (2011).

ONLINE METHODS

Reagents. Novartis provided LCL161 (refs. 21,22). SM-122 and SM-164 were provided by S. Wang (University of Michigan, USA)[39]. AEG40730 (ref. 40) was synthesized by Vibrant Pharma Inc. OICR720 was synthesized by the Ontario Institute for Cancer Research (OICR)[41]. IFN-α, IFN-β, IL-28 and IL-29 were obtained from PBL Interferonsource. All siRNAs were obtained from Dharmacon (ON-TARGETplus SMARTpool). CpG-ODN 2216 was synthesized by IDT (5′-gggGGACGATCGTCgggggg-3′, lowercase indicates phosphorothioate linkages between these nucleotides, whereas underlining identifies three CpG motifs with phosphodiester linkages). Imiquimod was purchased from BioVision Inc. poly(I:C) was obtained from Invivogen. LPS was from Sigma.

Cell culture. Cells were maintained at 37 °C and 5% CO_2 in DMEM media supplemented with 10% heat-inactivated FCS, penicillin, streptomycin and 1% nonessential amino acids (Invitrogen). All of the cell lines were obtained from ATCC, with the following exceptions: SNB75 (D. Stojdl, Children's Hospital of Eastern Ontario Research Institute) and SF539 (UCSF Brain Tumor Bank). Cell lines were regularly tested for mycoplasma contamination. For siRNA transfections, cells were reverse transfected with Lipofectamine RNAiMAX (Invitrogen) or DharmaFECT I (Dharmacon) for 48 h as per the manufacturer's protocol.

Viruses. The Indiana serotype of VSVΔ51 (ref. 42) was used in this study and was propagated in Vero cells. VSVΔ51-GFP is a recombinant derivative of VSVΔ51 expressing jelly fish green fluorescent protein. VSVΔ51–Fluc expresses firefly luciferase. VSVΔ51 with the deletion of the gene encoding for glycoprotein (VSVΔ51ΔG) was propagated in HEK293T cells that were transfected with pMD2-G using Lipofectamine 2000 (Invitrogen). To generate the VSVΔ51-TNF-α construct, full-length human TNF-α gene was inserted between the G and L viral genes. All VSVΔ51 viruses were purified on a sucrose cushion. Maraba-MG1, VVDD-B18R−, Reovirus and HSV1 ICP34.5 were generated as previously described[43–45]. Generation of adenoviral vectors expressing GFP or coexpressing GFP and dominant negative IKK-β was as previously described[16].

***In vitro* viability assay.** Cell lines were seeded in 96-well plates and incubated overnight. Cells were treated with vehicle (0.05% DMSO) or 5 µM LCL161 and infected with the indicated MOI of oncolytic virus or treated with 250 U/ml IFN-β, 500 U/ml IFN-α, 500 U/ml IFN-γ, 10 ng/ml IL-28 or 10 ng/ml IL-29 for 48 h. Cell viability was determined by Alamar blue (Resazurin sodium salt (Sigma))[46] and data were normalized to vehicle treatment. The chosen sample size is consistent with previous reports that used similar analyses for viability assays, but no statistical methods were used to determine sample size[15,16]. For combination indices (CI), cells were seeded overnight, treated with serial dilutions of a fixed combination mixture of VSVΔ51 and LCL161 (5,000:1, 1,000:1 and 400:1 ratios of PFU VSVΔ51: µM LCL161) for 48 h and cell viability was assessed by Alamar blue. CI were calculated according to the method of Chou and Talalay using Calcusyn[47]. An n = 3–4 of biological replicates was used to determine statistical measures (mean, s.d. or standard error).

Spreading assay. A confluent monolayer of 786-0 cells (human renal cell adenocarcinoma) was overlaid with 0.7% agarose in complete media. A small hole was made with a pipette in the agarose overlay in the middle of the well where 5×10^2 PFU of VSVΔ51-GFP was administered. Media containing vehicle or 5 µM LCL161 was added on top of the overlay, cells were incubated for 4 d, fluorescent images were acquired and cells were stained with crystal violet. An n = 3 of biological replicates was used to determine statistical measures (mean, s.d.)

Splenocyte coculture. EMT6 cells were cultured in multiwell plates and overlaid with cell culture transwell inserts containing unfractionated splenocytes. Single-cell splenocyte suspensions were obtained by passing mouse spleens through 70 µm nylon mesh, and red blood cells were lysed with ACK lysis buffer. Splenocytes were cotreated for 24 h with 1 µM LCL161 and 0.1 MOI of VSVΔ51ΔG, 1 µg/ml poly(I:C), 1 µg/ml LPS, 2 µM imiquimod or 0.25 µM CpG. EMT6 cell viability was determined by crystal violet

staining. An n = 3 of biological replicates was used to determine statistical measures (mean, s.d.).

Cytokine responsiveness bioassay. Cells were infected with the indicated MOI of VSVΔ51 for 24 h and the cell culture supernatant was exposed to UV light for 1 h to inactive VSVΔ51 particles. Subsequently, the UV-inactivated supernatant was applied to naive cells in the presence of 5 µM LCL161 for 48 h. Cell viability was assessed by Alamar blue. An n = 3 of biological replicates was used to determine statistical measures (mean, s.d.).

Microscopy. To determine the kinetics of VSVΔ51 spread, cells were infected with VSVΔ51-GFP and placed in an incubator outfitted with an IncuCyte Zoom microscope equipped with a 10× objective. Phase-contrast and fluorescence images of four fields per well were automatically acquired every 30 min over a span of 48 h. To visualize bystander cell death via immunofluorescence, cells were treated with 5 µM LCL161 and 0.01 MOI of VSVΔ51-GFP for 36 h and labeled with the Magic Red Caspase-3/7 Assay Kit (ImmunoChemistry Technologies). Images were acquired on an InCell Analyzer 6000 (GE). To measure the proportion of caspase-3/7 activity, 5 µM LCL161, the indicated MOI of VSVΔ51 and 5 µM CellPlayer Apoptosis Caspase-3/7 reagent (Essen Bioscience) was added to the cells. Cells were imaged with the IncuCyte Zoom. To measure the proportion of apoptotic cells, 1 µg/ml Annexin V-CF594 (Biotium) and 0.2 µM YOYO-1 (Invitrogen) was added to SMC and VSVΔ51 treated cells at 24 h post-treatment. Images were acquired using the IncuCyte Zoom. Enumeration of fluorescence signals from the IncuCyte Zoom was processed using the integrated object counting algorithm within the IncuCyte Zoom software. An n = 12 (VSVΔ51-GFP), n = 12 (caspase-3/7) or n = 9 (Annexin V, YOYO-1) of biological replicates was used to determine statistical measures (mean, s.d.).

Multiple step growth curves. Cells were treated with vehicle or 5 µM LCL161 for 2 h and subsequently infected at the indicated MOI of VSVΔ51 for 1 h. Cells were washed with PBS, replenished with media containing vehicle or 5 µM LCL161 and incubated at 37 °C. Aliquots were obtained at the indicated times and viral titers assessed by a standard plaque assay using African green monkey VERO cells.

Western blot analysis. Cells were scraped, collected by centrifugation and lysed in RIPA lysis buffer containing a protease inhibitor cocktail (Roche). Equal amounts of soluble protein were separated on polyacrylamide gels followed by transfer to nitrocellulose membranes. Individual proteins were detected by western blotting using the following antibodies: pSTAT1 (9171), caspase-3 (9661), caspase-8 (9746), caspase-9 (9508), DR5 (3696), TNF-R1 (3736), cFLIP (3210) and PARP (9541) from Cell Signaling Technology; caspase-8 (1612) from Enzo Life Sciences; IFNAR1 (EP899) and TNF-R1 (19139) from Abcam; caspase-8 (AHZ0502) from Invitrogen; cFLIP (clone NF6) from Alexis Biochemicals; RIP1 (clone 38) from BD Biosciences; and E7 from Developmental Studies Hybridoma Bank. Our rabbit anti-rat IAP1 and IAP3 polyclonal antibodies were used to detect human and mouse cIAP1/2 and XIAP, respectively[9]. Alexa Fluor 680 (Invitrogen) or IRDye800 (Li-Cor) were used to detect the primary antibodies, and infrared fluorescent signals were detected using the Odyssey Infrared Imaging System (Li-Cor). Full-length western blots are presented in **Supplementary Figure 19**.

RT-qPCR. Total RNA was isolated from cells using the RNAEasy Mini Plus kit (Qiagen). Two step RT-qPCR was performed using Superscript III (Invitrogen) and SsoAdvanced SYBR Green supermix (Bio-Rad) on a Mastercycler ep realplex (Eppendorf). All primers were obtained from realtimeprimers.com (**Supplementary Table 2**). An n = 3 of biological replicates was used to determine statistical measures (mean, s.d.).

ELISA. Cells were infected with virus at the indicated MOI or treated with IFN-β for 24 h, cell culture debris was removed by centrifugation and cytokines within the supernatant were measured with the TNF-α Quantikine high sensitivity, TNF-α DuoSet, TRAIL DuoSet (R&D Systems) or VeriKine IFN-β (PBL Interferonsource) assay kits. In some cases, the cell culture supernatants

were concentrated using Amicon Ultra filtration units. An $n = 3$ of biological replicates was used to determine statistical analysis (mean, s.d.).

EMT6 mammary tumor model. Mammary tumors were established by injecting 1×10^5 wild-type EMT6 or firefly luciferase-tagged EMT6 (EMT6-Fluc) cells in the mammary fat pad of 6-week-old female BALB/c mice. Mice with palpable tumors (~100 mm³) were cotreated with either vehicle (30% 0.1 M HCl, 70% 0.1 M NaOAc pH 4.63) or 50 mg/kg LCL161 orally and either i.v. injections of either PBS or 5×10^8 PFU of VSVΔ51 twice weekly for 2 weeks. For poly(I:C) and SMC treatments, animals were treated with LCL161 twice a week and either BSA (intratumoral (i.t.)), 20 μg poly(I:C) i.t. or 2.5 mg/kg poly(I:C) i.p. four times a week. The SMC and CpG group was injected with 2 mg/kg CpG (i.p.) and the next day was followed with CpG and SMC treatments. The CpG and SMC treatments were repeated 4 d later. Treatment groups were assigned by cages and each group had minimum 4–8 mice for statistical measures (mean, standard error; Kaplan-Meier with log-rank analysis). The sample size is consistent with previous reports that examined tumor growth and mouse survival following cancer treatment but no statistical methods were used to determine sample size[26,43,44]. Blinding was not possible. Animals were euthanized when tumors metastasized intraperitoneally or when the tumor burden exceeded 2,000 mm³. Tumor volume was calculated using $(\pi)(W)^2(L)/4$, where W = tumor width and L = tumor length. Tumor bioluminescence imaging was captured with a Xenogen2000 IVIS CCD-camera system (Caliper Life Sciences) following i.p. injection of 4 mg luciferin (Gold Biotechnology).

HT-29 subcutaneous tumor model. Subcutaneous tumors were established by injecting 3×10^6 HT-29 cells in the right flank of 6-week-old female CD-1 nude mice. Palpable tumors (~200 mm³) were treated with five i.t. injections of PBS or 1×10^8 PFU of VSVΔ51. Four hours later, mice were administered vehicle or 50 mg/kg LCL161 orally. Treatment groups were assigned by cages and each group had a minimum of 5–7 mice for statistical measures (mean, standard error; Kaplan-Meier with log-rank analysis). The sample size is consistent with previous reports that examined tumor growth and mouse survival following cancer treatment but no statistical measures were used to determine sample size[26,43,44]. Blinding was not possible. Animals were euthanized when tumor burden exceeded 2,000 mm³. Tumor volume was calculated using $(\pi)(W)^2(L)/4$, where W = tumor width and L = tumor length.

All animal experiments were conducted with the approval of the University of Ottawa Animal Care and Veterinary Service in concordance with guidelines established by the Canadian Council on Animal Care.

Antibody-mediated cytokine neutralization. For neutralizing TNF-α signaling *in vitro*, 25 μg/ml of α-TNF-α (XT3.11) or isotype control (HRPN) was added to EMT6 cells for 1 h before LCL161 and VSVΔ51 or IFN-β cotreatment for 48 h. Viability was assessed by Alamar blue. An $n = 3$ of biological replicates was used to determine statistical measures (mean, s.d.). For neutralizing TNF-α in the EMT6-Fluc tumor model, 0.5 mg of TNF-α or HRPN was administered i.p. 8, 10 and 12 d post-implantation. Mice were treated with 50 mg/kg LCL161 (oral) on 8, 10 and 12 d post-implantation and were infected with 5×10^8 PFU VSVΔ51 i.v. on days 9, 11 and 13. Treatment groups were assigned by cages and each group had minimum 4–8 mice for statistical measures (mean, standard error; Kaplan-Meier with log-rank analysis). The sample size is consistent with previous reports that examined tumor growth and mouse survival following cancer treatment but no statistical methods were used to determine sample size[26,43,44]. Blinding was not possible. Animals were euthanized when tumors metastasized intraperitoneally or when the tumor burden exceeded 2,000 mm³. Tumor volume was calculated using $(\pi)(W)^2(L)/4$, where W = tumor width and L = tumor length. For neutralization of type I IFN signaling, 2.5 mg of IFNAR1 (MAR1-5A3) or isotype control (MOPC-21) were injected i.p. into EMT6-tumor bearing mice and treated with 50 mg/kg LCL161 (oral) for 20 h. Mice were infected with 5×10^8 PFU VSVΔ51 (i.v.) for

18–20 h and tumors were processed for western blot analysis. All antibodies were from BioXCell.

Flow cytometry and sorting. EMT6 cells were cotreated with 0.1 MOI of VSVΔ51-GFP and 5 μM LCL161 for 20 h. Cells were trypsinized, permeabilized with the CytoFix/CytoPerm kit (BD Biosciences) and stained with APC-TNF-α (MP6-XT22, BD Biosciences). Cells were analyzed on a Cyan ADP 9 flow cytometer (Beckman Coulter) and data were analyzed with FlowJo (Tree Star).

Splenocytes were enriched for CD11b using the EasySep CD11b positive selection kit (StemCell Technologies). CD49$^+$ cells were enriched using the EasySep CD49b positive selection kit (StemCell Technologies) from the CD11b$^-$ fraction. CD11b$^+$ cells were stained with F4/80-PE-Cy5 (BM8, eBioscience) and Gr1-FITC (RB6-8C5, BD Biosciences) and further sorted with MoFlo Astrios (Beckman Coulter). Flow cytometry data were analyzed using Kaluza (Beckman Coulter). Isolated cells were infected with VSVΔ51 for 24 h and clarified cell culture supernatants were applied to EMT6 cells for 24 h in the presence of 5 μM LCL161. An $n = 3$ of biological replicates was used to determine statistical measures (mean, s.d.).

Bone marrow–derived macrophages. Mouse femurs and radii were removed and flushed to remove bone marrow. Bone marrow cells were cultured in Petri dishes with RPMI, 8% FBS and 5 ng/ml of M-CSF for 7 d. Flow cytometry was used to confirm the purity of the adherent macrophages (F4/80$^+$ CD11b$^+$).

Immunohistochemistry. Excised tumors were fixed in 4% PFA, embedded in a 1:1 mixture of OCT compound and 30% sucrose, and sectioned on a cryostat at 12 μm. Sections were permeabilized with 0.1% Triton X-100 in blocking solution (50 mM Tris–HCl pH 7.4, 100 mM L-lysine, 145 mM NaCl and 1% BSA, 10% goat serum). α-cleaved caspase 3 (C92-605, BD Pharmingen) and polyclonal antiserum VSV (Earl Brown, University of Ottawa, Canada) were incubated overnight followed by secondary incubation with Alexa Fluor–coupled secondary antibodies (Invitrogen).

Statistical analysis. Comparison of Kaplan-Meier survival plots was conducted by log-rank analysis and subsequent pairwise multiple comparisons were performed using the Holm-Sidak method (SigmaPlot). Calculation of EC_{50} values was performed in GraphPad Prism using normalized nonlinear regression analysis (variable slope). The EC_{50} shift was calculated by subtracting the $\log_{10} EC_{50}$ of SMC-treated and VSVΔ51-infected cells from $\log_{10} EC_{50}$ of vehicle-treated cells infected by VSVΔ51. To normalize the degree of SMC synergy, the EC_{50} value was scaled to 100% to compensate for cell death induced by SMC treatment alone.

39. Sun, H. *et al.* Design, synthesis, and characterization of a potent, nonpeptide, cell-permeable, bivalent Smac mimetic that concurrently targets both the BIR2 and BIR3 domains in XIAP. *J. Am. Chem. Soc.* **129**, 15279–15294 (2007).
40. Bertrand, M.J. *et al.* cIAP1 and cIAP2 facilitate cancer cell survival by functioning as E3 ligases that promote RIP1 ubiquitination. *Mol. Cell* **30**, 689–700 (2008).
41. Enwere, E.K. *et al.* TWEAK and cIAP1 regulate myoblast fusion through the noncanonical NF-kappaB signalling pathway. *Sci. Signal.* **5**, ra75 (2012).
42. Stojdl, D.F. *et al.* VSV strains with defects in their ability to shutdown innate immunity are potent systemic anti-cancer agents. *Cancer Cell* **4**, 263–275 (2003).
43. Brun, J. *et al.* Identification of genetically modified Maraba virus as an oncolytic rhabdovirus. *Mol. Ther.* **18**, 1440–1449 (2010).
44. Le Boeuf, F. *et al.* Synergistic interaction between oncolytic viruses augments tumour killing. *Mol. Ther.* **18**, 888–895 (2010).
45. Lun, X. *et al.* Efficacy and safety/toxicity study of recombinant vaccinia virus JX-594 in two immunocompetent animal models of glioma. *Mol. Ther.* **18**, 1927–1936 (2010).
46. Mikus, J. & Steverding, D. A simple colorimetric method to screen drug cytotoxicity against Leishmania using the dye Alamar Blue. *Parasitol. Int.* **48**, 265–269 (2000).
47. Chou, T.C. & Talaly, P. A simple generalized equation for the analysis of multiple inhibitions of Michaelis-Menten kinetic systems. *J. Biol. Chem.* **252**, 6438–6442 (1977).